Deadbeat Predictive Current Control of DC-Biased-VRM Based on Extended State Observer With Coupling Disturbance Compensation

Zixiang Yu, *Member, IEEE*, Xiang Zhang, Jiwen Zhao, *Senior Member, IEEE*, Yuhang Chen, Zhenbao Pan, *Member, IEEE*, and Lijun Wang, *Member, IEEE*

***Abstract*—This article proposes a deadbeat predictive current control (DPCC) of dc-biased Vernier reluctance machine (dc-biased-VRM) based on extended state observer (ESO) with coupling disturbance compensation to improve the dynamic response and disturbance resistance ability of the control system. Firstly, the DPCC strategy was introduced into dc-biased-VRM, and the ESO-based DPCC method that ignores coupling was obtained. On this basis, the impacts of parameter mismatch and coupling disturbance of dc-biased-VRM on DPCC are analyzed, and an ESO with coupling disturbance compensation is proposed, which can swiftly compensate the disturbances arising from parameter mismatch and coupling effects. Furthermore, a quasi-resonant controller was introduced to suppress the harmonic current of the machine. Ultimately, the accuracy of current prediction and the dynamic response ability of current were improved, and this proposed strategy has a better ability to resist disturbances. Finally, by comparing the experimental results of the proposed strategy with those of the conventional one, the conclusion of this article was verified.**

***Index Terms*—Coupling disturbance compensation, dc-biased-Vernier reluctance machine (VRM), deadbeat predictive current control (DPCC), extended state observer (ESO).**

I. Introduction

THE internal aviation starter/generator is the core component of the multielectric aircraft electrical system. The location of the internal starter/generator is harsh and the temperature is high, which puts forward higher requirements for the machine reliability. At the same time, how to control the start and power generation process of the starter/generator machine to achieve high real-time and stable control, has also received increasing attention in recent years [1], [2].

The switched reluctance machine (SRM) is simple in structure and reliable in operation, suitable for application in internal aviation starter/generator [3]. However, SRM also has the problems of complicated power generation control with low precision, and serious vibration. For the improvement needs of SRM, a novel type of machine named dc-biased-Vernier reluctance machine (VRM) has been developed [4], [5]. This machine adopts an open winding inverter to ensure that both dc and ac current exist in the armature winding [6]. It retains the characteristics of SRM double salient poles, thereby ensuring more stable and reliable operation. Without the employment of permanent magnet materials, there is no risk of demagnetization in high-temperature environments. The use of smoother sinusoidal ac current also contributes to reducing motor vibration and noise. Combined with the integrated current vector control strategy, it improves the power generation control accuracy [7], [8], [9]. Meanwhile, the flexible distribution of dc bias current makes the machine have good speed regulation performance and starting characteristics [10], [11]. The application of two inverters also brings more convenience for fault tolerant control [12], [13]. These characteristics make the machine suitable for applications such as automotive turbocharging and mining machinery, especially in harsh environments with high temperatures, high speeds, and strong vibrations. However, these application scenarios also place high demands on the dynamic performance of the machine system.

Based on the optimal design of the machine, the system performance can be further improved by optimizing the control strategy. The dc-biased-VRM initially uses PI regulator to realize current control of $dq0$-axis, but the dynamic response of PI control system is slow. To address this problem, some scholars have proposed the DPCC strategy and successfully applied it in permanent magnet synchronous machine (PMSM) drive system [14], [15], this method has good dynamic performance and can adjust the error in a short time. However, the dynamic and steady state performance of DPCC is heavily reliant on the accuracy of machine parameters. In the actual control system, it is inevitable that machine parameters will change, which will seriously affect the control effect of DPCC strategy [16].

In order to further improve the application range of the DPCC strategy, Liu et al. [17] extend the prediction range to the

Received 22 June 2025; revised 11 October 2025; accepted 16 November 2025. Date of publication 24 November 2025; date of current version 25 February 2026. This work was supported in part by the National Natural Science Foundation of China under Grant 52577047, Grant 52207044, and Grant U23A20644, and in part by the Fundamental Research Funds for the Central Universities under Grant JZ2024HGTB0227. Recommended for publication by Associate Editor J. Hur. *(Corresponding author: Jiwen Zhao.)*

Zixiang Yu, Xiang Zhang, Jiwen Zhao, Yuhang Chen, and Zhenbao Pan are with the School of Electrical Engineering and Automation, Hefei University of Technology, Hefei 230009, China. (e-mail: zixiangyu@hfut.edu.cn; xiangzhang@mail.hf-ut.edu.cn; ustczjw@hfut.edu.cn; 2023170461@mail.hfut.edu.cn; pzhenbao@hfut.edu.cn).

Lijun Wang is with the School of Internet, Anhui University, Hefei 230009, China. (e-mail: lijun-wang@ahu.edu.cn).

Color versions of one or more figures in this article are available at https://doi.org/10.1109/TPEL.2025.3635945.

Digital Object Identifier 10.1109/TPEL.2025.3635945

whole dynamic range of the transient state, which realizes the optimization of the stator voltage angle and improves the stable operating range when the inductance is mismatched. By introducing integrated sliding mode control, Xu et al. [18] improve the system's immunity to centralized disturbance. In addition, many scholars also use observers to improve the resistance of DPCC strategies. Sun et al. [19] designed a stator current and lumped disturbance observer to effectively reduce the impact of parameter mismatch. However, the above method does not take zero-sequence current into account, so some scholars have designed three-dimensional DPCC for open winding permanent magnet synchronous machine. Zhang and Zhang [20] proposes a zero-sequence reference voltage reallocation strategy to achieve complete suppression of zero-sequence current. Yuan et al. [21] propose a full-order adaptive zero-sequence observer to predict the future zero-sequence current and zero-sequence voltage, and successfully compensates the control delay. Li et al. [22] extend the ESO to 0-axis and uses the predicted disturbance as feedforward compensation for DPCC to enhance the robustness of the control system. Due to the additional control requirement for zero-sequence current to achieve stator excitation, the above-mentioned DPCC strategies are not applicable to dc-biased-VRM. In addition, the coupling effect complicates the voltage equation of the $dq0$-axis. Observing and compensating for the interference caused by this coupling to achieve efficient control of the current along the $dq0$-axis can further enhance the dynamic response capability and control effect of the system. Therefore, none of the above methods can be directly applied to dc-biased-VRM.

In view of the shortcomings of the existing DPCC strategy and the necessity for high dynamic response capability in the dc-biased-VRM control system, a deadbeat predictive current control (DPCC) of dc-biased-VRM based on extended state observer (ESO) with coupling disturbance compensation is proposed in this article.

The rest of this article is organized as follows. In Section II, the features of dc-biased-VRM are introduced. In Section III, the DPCC strategy is introduced into dc-biased-VRM, and a conventional ESO-based DPCC strategy that ignores coupling is designed. In Section IV, the coupling phenomenon of dc-biased-VRM and the influence of parameter mismatch are further analyzed, and an improved DPCC of dc-biased-VRM based on ESO with coupling disturbance compensation is proposed. In Section V, experimental comparisons are conducted to assess the control performance of the two control strategies proposed in this article, thereby verifying the superiority of the proposed strategies. Finally, Section VI concludes this article.

II. Structure and Principle of DC-Biased-VRM

Fig. 1(a) and (b) depicts the stator-rotor structure and winding connection of dc-biased-VRM with 12-stator 10-rotor, respectively. The stator and rotor of the machine feature a salient pole structure, and the stator is additionally equipped with a centralized winding. Each end of this winding is connected to an inverter, allowing a zero-sequence current to flow through it. The current in the winding can be expressed as (1). I_0 is the amplitudes of zero-sequence current, I_1 is the amplitude of the

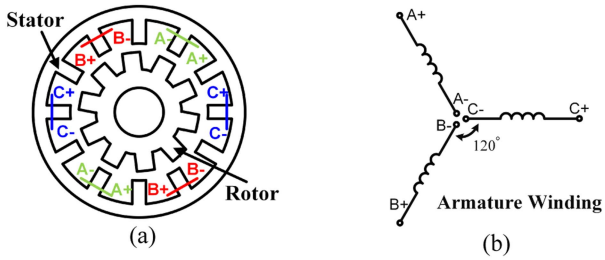

Fig. 1 DC-biased-VRM. (a) Topology. (b) Winding connection.

fundamental current, and θ_e is the electrical angle

$$\begin{cases} i_a = I_0 + I_1\cos(\theta_e) \\ i_b = I_0 + I_1\cos(\theta_e - 2/3\pi) \\ i_c = I_0 + I_1\cos(\theta_e + 2/3\pi) \end{cases}. \tag{1}$$

The inductance is primarily comprised of the dc component L_0 and the primary alternating component L_1, with the amplitudes of other components being insignificant and thus disregarded. Therefore, the phase inductance is represented as [23]

$$\begin{cases} L_a = L_0 + L_1\cos(\theta_e) \\ L_b = L_0 + L_1\cos(\theta_e - 2/3\pi) \\ L_c = L_0 + L_1\cos(\theta_e + 2/3\pi) \end{cases}. \tag{2}$$

For dc-biased-VRM, the voltage equation in the three-phase stationary coordinate system can be expressed as (3). In (3), R_s is the resistance of stator windings. i_{abc} is the phase currents, L_{abc} is the inductances

$$u_{abc} = R_s i_{abc} + \frac{d(L_{abc} i_{abc})}{dt}. \tag{3}$$

PARK transformation can be used to transform (1) and (2) into the $dq0$-axis frame, and the electrical angle of the transformation is θ_e. Then using (3), the voltage equation in the $dq0$-axis can be obtained, as shown in [10]

$$\begin{bmatrix} u_d \\ u_q \\ u_0 \end{bmatrix} = R_s \begin{bmatrix} i_d \\ i_q \\ i_0 \end{bmatrix} + \begin{bmatrix} L_0 & 0 & L_1 \\ 0 & L_0 & 0 \\ L_1/2 & 0 & L_0 \end{bmatrix} \begin{bmatrix} di_d/dt \\ di_q/dt \\ di_0/dt \end{bmatrix} + \omega_e \begin{bmatrix} 0 & -L_0 & 0 \\ L_0 & 0 & L_1 \\ 0 & 0 & 0 \end{bmatrix} \begin{bmatrix} i_d \\ i_q \\ i_0 \end{bmatrix}. \tag{4}$$

The ac current generates stator flux, while the dc current produces virtual rotor flux. Electromagnetic torque is generated through the interaction between stator and rotor fluxes, driving the machine to operate. The average electromagnetic torque in dc-biased-VRM is proportional to the product of i_q and i_0 [11].

III. Conventional ESO-Based DPCC Strategy for DC-Biased-VRM That Ignores Coupling

The DPCC strategy is widely applied in PMSM drive systems and does not require consideration of the coupling terms that exist in systems like dc-biased-VRM. To apply the DPCC strategy to dc-biased-VRM, a traditional and simplified DPCC strategy was derived with reference to the DPCC strategy used in PMSM. In general, if the sampling time is fairly short, the forward Euler method can be used to discretize (4) [17]. To

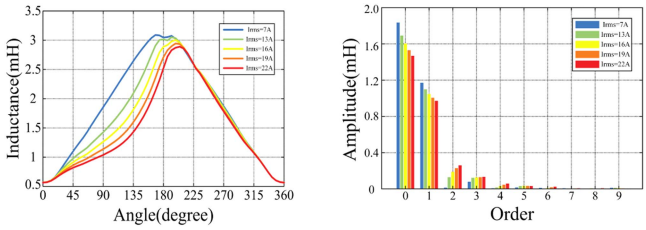

Fig. 2 Example of DC-biased-VRM inductance changing with $I_{\rm rms}$. (a) Inductance. (b) FFT analysis of inductance.

compare with the strategy considering coupling effects, the coupling terms are first ignored following the DPCC strategy for PMSM. Specifically, the term $L_1 di_0/dt$ is neglected in the d-axis, and the term $0.5L_1 di_d/dt$ is neglected in the 0-axis. The handling of coupling terms in dc-biased-VRM constitutes the main contribution of this article. Ignoring these coupling terms facilitates the comparison of experimental results between the traditional strategy and the coupling disturbance compensation strategy proposed in this article. However, the coupling disturbances caused by sudden changes in motor current cannot be effectively addressed, which in turn affects the dynamic performance of current regulation. A more effective improved method will be introduced in Section IV.

In this case (4) can be represented as (5). Then discretize (5) to obtain (6) shown at the bottom of this page. In (6), $i_d(k)$, $i_q(k)$, and $i_0(k)$ represent the sampled current of the $dq0$-axis at the ongoing control period, respectively. T_s is the control period. Then, the current of the $dq0$ axis for the next control cycle is predicted based on the machine parameters, as shown in (7). Given that the control period is exceedingly brief, ω_e between two consecutive periods can be deemed as remaining constant

$$\begin{bmatrix} u_d \\ u_q \\ u_0 \end{bmatrix} = R_s \begin{bmatrix} i_d \\ i_q \\ i_0 \end{bmatrix} + \begin{bmatrix} L_0 & 0 & 0 \\ 0 & L_0 & 0 \\ 0 & 0 & L_0 \end{bmatrix} \begin{bmatrix} di_d/dt \\ di_q/dt \\ di_0/dt \end{bmatrix} + \omega_e \begin{bmatrix} 0 & -L_0 & 0 \\ L_0 & 0 & L_1 \\ 0 & 0 & 0 \end{bmatrix} \begin{bmatrix} i_d \\ i_q \\ i_0 \end{bmatrix} \tag{5}$$

To ensure that the machine's feedback current follows its corresponding reference value, it's crucial to predict the current value for the next control cycle during the ongoing control cycle. This predicted value is then used as the feedback current for the subsequent control cycle. Based on this reference, the regulation voltage for the next control cycle is computed. This regulation voltage is implemented on the machine at the beginning of each control period, enabling precise adjustments to the current so that it reaches the desired value by the end of that period. The regulation voltage can be obtained from (8)

$$\begin{cases} \hat{i}_d(k+1) = (1 - \frac{RT_s}{L_0}) i_d(k) + \frac{T_s}{L_0} U_d(k) + T_s \omega_e(k) i_q(k) \\ \hat{i}_q(k+1) = (1 - \frac{RT_s}{L_0}) i_q(k) + \frac{T_s}{L_0} U_q(k) - T_s \omega_e(k) i_d(k) \\ -T_s \omega_e(k) \frac{L_1}{L_0} i_0(k) \\ \hat{i}_0(k+1) = (1 - \frac{RT_s}{L_0}) i_0(k) + \frac{T_s}{L_0} U_0(k) \end{cases} \tag{7}$$

$$\begin{cases} u_d(k+1) = R\hat{i}_d(k+1) + \frac{L_0}{T_s}(i_{\rm dref}(k+1) - \hat{i}_d(k+1)) \\ -L_0 \omega_e(k) \hat{i}_q(k+1) \\ u_q(k+1) = R\hat{i}_q(k+1) + \frac{L_0}{T_s}(i_{\rm qref}(k+1) - \hat{i}_q(k+1)) \\ +L_0 \omega_e \hat{i}_d(k+1) + L_1 \omega_e(k) \hat{i}_0(k+1) \\ u_0(k+1) = R\hat{i}_0(k+1) + \frac{L_0}{T_s}(i_{0\rm ref}(k+1) - \hat{i}_0(k+1)) \end{cases} \tag{8}$$

In order to enhance the robustness of DPCC against interference and minimize the effects of parameter variations, an ESO is designed to detect and compensate for the disturbances that arise due to parameter mismatch. Zhang et al. [24] provide a discretization formula for ESO, as shown in (9), where $e_{rr}(k)$ represents the difference between the predicted value and the feedback value of the current.

According to (7) and (9), the design of the ESO can be expressed as (10) and (11). In (10) and (11), $f_d(k+1)$, $f_q(k+1)$ and $f_0(k+1)$ represent the predicted $dq0$-axis current disturbance, respectively, a_d, b_d, a_q, b_q, a_0, and b_0 are parameters of ESO. Finally, the reference voltage after disturbance compensation can be expressed as shown in (12)

$$\begin{cases} e_{rr}(k) = \hat{i}(k) - i(k) \\ \hat{i}(k+1) = \hat{i}(k) + T_s(u(k) + f(k)) - a \cdot e_{rr}(k) \\ f(k+1) = f(k) - b \cdot e_{rr}(k) \end{cases} \tag{9}$$

$$\begin{cases} \hat{i}_d(k+1) = \frac{T_s}{L_0}(U_d(k) - R\hat{i}_d(k) + L_0 \omega_e(k) i_q(k)) + \hat{i}_d(k) \\ -T_s \cdot a_d \cdot (\hat{i}_d(k) - i_d(k)) + f_d(k) T_s \\ \hat{i}_q(k+1) = \frac{T_s}{L_0}(U_q(k) - R\hat{i}_q(k) - L_0 \omega_e(k) i_d(k) + f_q(k) T_s \\ -L_1 \omega_e(k) i_0(k)) + \hat{i}_q(k) - T_s \cdot a_q \cdot (\hat{i}_q(k) - i_q(k)) \\ \hat{i}_0(k+1) = \frac{T_s}{L_0}(U_0(k) - R\hat{i}_0(k)) - T_s \cdot a_0 \cdot (\hat{i}_0(k) - i_0(k)) \\ +\hat{i}_0(k) + f_0(k) T_s \end{cases} \tag{10}$$

$$\begin{cases} f_d(k+1) = -T_s \cdot b_d \cdot (\hat{i}_d(k) - i_d(k)) + f_d(k) \\ f_q(k+1) = -T_s \cdot b_q \cdot (\hat{i}_q(k) - i_q(k)) + f_q(k) \\ f_0(k+1) = -T_s \cdot b_0 \cdot (\hat{i}_0(k) - i_0(k)) + f_0(k) \end{cases} . \tag{11}$$

In this section, the conventional DPCC strategy with ESO for PMSM is taken as a reference and is introduced into the dc-biased-VRM control system, aiming to enhance the dynamic response capability of the dc-biased-VRM and reduce phase current ripple during current step changes. Experimental results validate the correctness of the theoretical derivation. Specifically, to facilitate direct application to the dc-biased-VRM, a simplified DPCC strategy with zero-sequence current regulation

$$\begin{bmatrix} u_d(k) \\ u_q(k) \\ u_0(k) \end{bmatrix} = R_s \begin{bmatrix} i_d(k) \\ i_q(k) \\ i_0(k) \end{bmatrix} + \begin{bmatrix} L_0 & 0 & 0 \\ 0 & L_0 & 0 \\ 0 & 0 & L_0 \end{bmatrix} \begin{bmatrix} (i_d(k+1) - i_d(k))/T_s \\ (i_q(k+1) - i_q(k))/T_s \\ (i_q(k+1) - i_q(k))/T_s \end{bmatrix} + \omega_e(k) \begin{bmatrix} 0 & -L_0 & 0 \\ L_0 & 0 & L_1 \\ 0 & 0 & 0 \end{bmatrix} \begin{bmatrix} i_d(k) \\ i_q(k) \\ i_0(k) \end{bmatrix} . \tag{6}$$

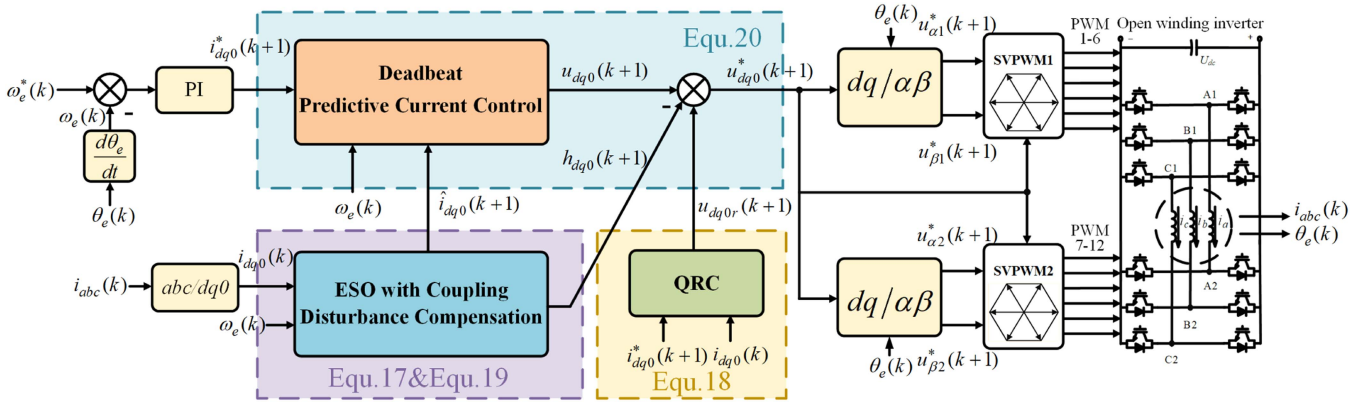

Fig. 3 Schematic diagram of the proposed strategy.

capability is derived by neglecting the additional derivative terms $L_1 di_0/dt$ and $0.5L_1 di_d/dt$, which would otherwise increase the algorithm complexity. However, these neglected terms are the source of the coupling in (4). This coupling phenomenon introduces disturbances between the predicted current and the compensation voltage, thereby degrading the dynamic performance of the control strategy. Therefore, the following section will investigate the effects of coupling and machine parameter mismatch on the control strategy, along with corresponding solutions

$$\begin{cases} u_d^*(k+1) = R\hat{i}_d(k+1) + \frac{L_0}{T_s}(i_{\mathrm{dref}}(k+1) - \hat{i}_d(k+1)) \\ -L_0\omega_e(k)\hat{i}_q(k+1) - f_d(k+1)L_0 \\ u_q^*(k+1) = R\hat{i}_q(k+1) + \frac{L_0}{T_s}(i_{\mathrm{qref}}(k+1) - \hat{i}_q(k+1)) \\ +L_0\omega_e(k)\hat{i}_d(k+1) - f_q(k+1)L_0 \\ +L_1\omega_e(k)\hat{i}_0(k+1) \\ u_0^*(k+1) = R\hat{i}_0(k+1) + \frac{L_0}{T_s}(i_{0\mathrm{ref}}(k+1) - \hat{i}_0(k+1)) \\ -f_0(k+1)L_0 \end{cases} \tag{12}$$

IV. Proposed DPCC of DC-Biased-VRM Based on ESO With Coupling Disturbance Compensation

A. Analysis of the Influence of Current Coupling and Machine Parameter Mismatch

The parameters of dc-biased-VRM change obviously in the actual system. As shown in Fig. 2, both the static inductance component and the alternating inductance component exhibit changes in response to variations in the root mean square of current (I_{rms}). In addition, in practical applications, ambient temperature fluctuations are inevitable, leading to corresponding changes in the machine's phase resistance as the temperature varies.

The variations in the static inductance component and alternating inductance component are expressed by ΔL_0 and ΔL_1, and the variation of phase resistance is expressed by ΔR. Consequently, the predicted current error induced by these machine parameter mismatch can be expressed as (13). According to (7), the predicted current in the case of parameter mismatch can be obtained, as shown in (14). The predicted current disturbances arising from the parameter variations at time k are expressed as $i_{fd}(k)$, $i_{fq}(k)$ and $i_{f0}(k)$. It is evident that variations in machine parameters will compromise the accuracy of current prediction, leading to errors in the regulating voltage, ultimately impacting the control effectiveness and potentially causing system instability. Hence, it is imperative to reduce the influence of parameter variations on control performance.

Furthermore, it is evident from (4) that the voltage on the $d0$-axis is related to the current of $d0$-axis, which means that the accuracy of the current prediction for the $d0$-axis directly influences the accuracy of the regulated voltage on the $dq0$-axis, subsequently impacting the control efficacy. However, in order to apply the conventional method to dc-biased-VRM, the coupling term di_0/dt of the d-axis and the coupling term di_d/dt of the 0-axis

TABLE I
Parameters of the Prototype DC-Biased-VRM

Parameters	Description	Value
n_s	Number of stator slot	12
n_r	Number of rotor slot	10
R_s	Phase resistance (Ω)	0.088
L_0	Static inductance component (mH)	1.53
L_1	Alternating inductance component (mH)	1.01
i_{sN}	Rated current (A)	19
T_{eN}	Rated torque (N·m)	2.55
n_N	Rated speed (r/min)	1500

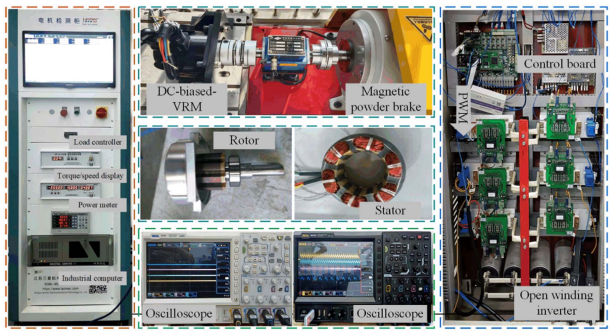

Fig. 4 DC-biased-VRM experiment platform.

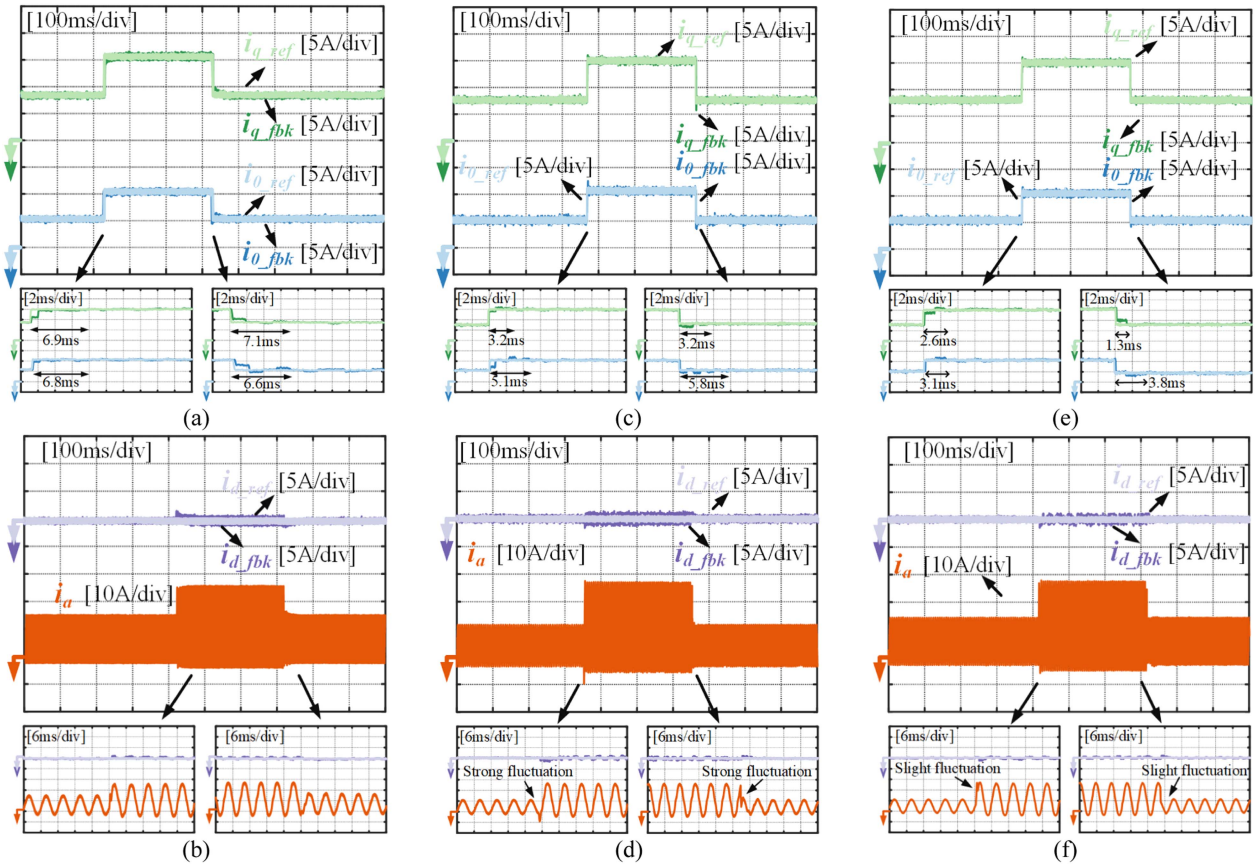

Fig. 5 Experimental results of dynamic response of *dq*0-axis current and phase current with different strategies. (a) i_q and i_0 of conventional VC strategy. (b) i_d and i_a of conventional VC strategy. (c) i_q and i_0 of conventional DPCC strategy. (d) i_d and i_a of conventional DPCC strategy. (e) i_q and i_0 of proposed DPCC strategy. (f) i_d and i_a of proposed DPCC strategy.

are neglected. This implies that the coupling phenomenon of the *dq*0-axis will introduce disturbances to the calculation of the predicted current and the given voltage value, ultimately affecting the dynamic performance of the control strategy. Moreover, variations in machine parameters further degrade the control performance, enhance this coupling effect

$$\begin{cases} \Delta\hat{i}_d(k+1) = (1-\frac{\Delta R T_s}{\Delta L_0}) i_d(k) + \frac{T_s}{\Delta L_0} U_d(k) \\ +T_s\omega_e(k) i_q(k) \\ \Delta\hat{i}_q(k+1) = (1-\frac{\Delta R T_s}{\Delta L_0}) i_q(k) + \frac{T_s}{\Delta L_0} U_q(k) \\ -T_s\omega_e(k) i_d(k) \\ -T_s\omega_e(k)\frac{\Delta L_1}{\Delta L_0} i_0(k) \\ \Delta\hat{i}_0(k+1) = (1-\frac{\Delta R T_s}{\Delta L_0}) i_0(k) + \frac{T_s}{\Delta L_0} U_0(k) \end{cases} \tag{13}$$

$$\begin{cases} \hat{i}_d(k+1) = (1-\frac{R*T_s}{L_0}) * i_d(k) + \frac{T_s}{L_0} U_d(k) \\ +T_s * \omega_e(k) * i_q(k) + i_{fd}(k) \\ \hat{i}_q(k+1) = (1-\frac{R*T_s}{L_0}) * i_q(k) + \frac{T_s}{L_0} U_q(k) \\ -T_s * \omega_e(k) * i_d(k) \\ -T_s * \omega_e(k) * \frac{L_1}{L_0} * i_0(k) + i_{fq}(k) \\ \hat{i}_0(k+1) = (1-\frac{R*T_s}{L_0}) * i_0(k) + \frac{T_s}{L_0} U_0(k) + i_{f0}(k) \end{cases} \tag{14}$$

Therefore, in this section, an ESO considering voltage coupling on the *dq*0-axis is designed. This strategy expands the coupling situation and parameter variations of the *dq*0-axis into disturbance quantities and observes them. Ultimately, it achieves disturbance compensation and enhances the dynamic performance of the control strategy.

B. Proposed ESO-Based DPCC Strategy With Coupling Disturbance Compensation

First, rewrite (4) as

$$\begin{bmatrix} u_d \\ u_q \\ u_0 \end{bmatrix} = R_s \begin{bmatrix} i_d \\ i_q \\ i_0 \end{bmatrix} + A \begin{bmatrix} di_d/dt \\ di_q/dt \\ di_0/dt \end{bmatrix} + \omega_e B \begin{bmatrix} i_d \\ i_q \\ i_0 \end{bmatrix} \tag{15}$$

In (15), $A = \begin{bmatrix} L_0 & 0 & L_1 \\ 0 & L_0 & 0 \\ L_1/2 & 0 & L_0 \end{bmatrix}$, $B = \begin{bmatrix} 0 & -L_0 & 0 \\ L_0 & 0 & L_1 \\ 0 & 0 & 0 \end{bmatrix}$.

In order to obtain the predicted current perturbations due to parameter mismatch and coupling phenomena, the differential value of the current in the *dq*0-axis is expressed as

$$\begin{bmatrix} di_d/dt \\ di_q/dt \\ di_0/dt \end{bmatrix} = D \begin{bmatrix} u_d + h_d \\ u_q + h_q \\ u_0 + h_0 \end{bmatrix} - D(R_s E + \omega_e B) \begin{bmatrix} i_d \\ i_q \\ i_0 \end{bmatrix}. \tag{16}$$

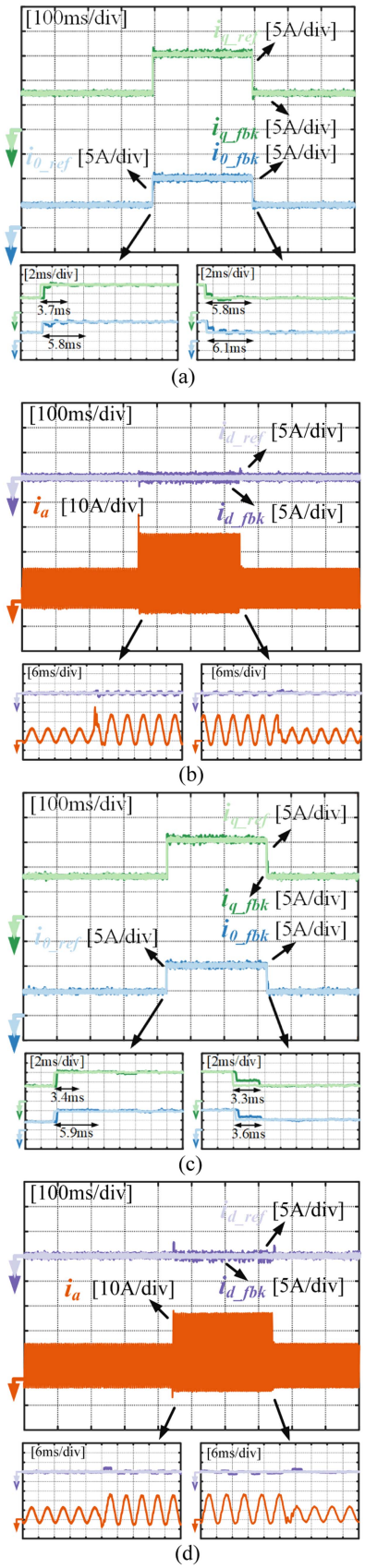

Fig. 6 Experimental results of dynamic responses of $dq0$-axis current and phase current with different strategies when parameters are mismatched. (a) i_q and i_0 of conventional DPCC strategy. (b) i_d and i_a of conventional DPCC strategy. (c) i_q and i_0 of proposed DPCC strategy. (d) i_d and i_a of proposed DPCC strategy.

In (16), $D = \begin{bmatrix} \frac{2L_0}{2L_0^2-L_1^2} & 0 & \frac{-2L_1}{2L_0^2-L_1^2} \\ 0 & \frac{1}{L_0} & 0 \\ \frac{-L_1}{2L_0^2-L_1^2} & 0 & \frac{2L_0}{2L_0^2-L_1^2} \end{bmatrix}$, $\boldsymbol{E}$ is the identity matrix, while h_d, h_q and h_0 denote the disturbance voltages that considering the coupling and parameter variations of the $dq0$-axis, respectively. According to (16), design considerations for ESO with coupling compensation can be expressed as (17).

Through (17), the coupling disturbance and parameter mismatch disturbance on the $dq0$-axis can be calculated, because when these two disturbances are obtained, not only the current of the d-axis is used, but also the influence of the current of the $q0$-axis on the d-axis is considered. For the 0-axis, the coupling disturbance caused by the current of d-axis on the 0-axis is also considered. In this way, the disturbance caused by the coupling phenomenon can be obtained separately. Furthermore, A quasi-resonant controller (QRC) is adopted to suppress the harmonic components in the back-electromotive force of dc-biased-VRM, thereby achieving harmonic current suppression. The QRC has been widely applied in suppressing alternating components [25], and the QRC used in this article is expressed as (18).

The expression for predicting the current can be expressed as (19) shown at the bottom of the next page. In (19), the coupling disturbance and parameter mismatch disturbance obtained in (17) are used to predict the next period current, which can improve the accuracy of current prediction in the transient process, and thus improve the transient control effect. After the predicted current and current disturbance, as well as the harmonic compensation voltage are obtained, the regulation voltage can be expressed as (20) shown at the bottom of the next page. The harmonic compensation voltages of the $dq0$-axis are represented as u_{dr}, u_{qr}, and u_{0r}, respectively. Besides, QRC has also been applied in the conventional DPCC method.

Fig. 3 shows the schematic diagram of the proposed strategy. When designing the ESO for the conventional DPCC method, the coupling phenomenon of dc-biased-VRM was ignored. This simplified approach enables rapid current regulation, but there is still room for improvement in dynamic processes. However, in Fig. 3, the proposed method, when designing the ESO, not only takes into account the disturbances caused by parameter variations but also comprehensively considers the coupling disturbances arising from current changes in the $dq0$-axes. Through the prediction of both the current and disturbance voltage, a compensation for the control delay is achieved. Additionally, the influence exerted by voltage coupling and parameter disturbance is mitigated, thereby ensuring the swift responsiveness and stability of the control system

$$\begin{bmatrix} h_d(k+1) \\ h_q(k+1) \\ h_0(k+1) \end{bmatrix} = -T_s D \begin{bmatrix} b_d(\hat{i}_d(k) - i_d(k)) \\ b_q(\hat{i}_q(k) - i_q(k)) \\ b_0(\hat{i}_0(k) - i_0(k)) \end{bmatrix} + \begin{bmatrix} h_d(k) \\ h_q(k) \\ h_0(k) \end{bmatrix} \quad (17)$$

$$G_{qrc}(s) = \frac{2k_p\omega_c s}{s^2 + 2\omega_c s + \omega_{qrc}^2}. \quad (18)$$

V. Experimental Verification

To validate the efficacy of the two strategies in enhancing the current response of the machine, an experiment is carried

out on the dc-biased-VRM experiment platform. Fig. 4 shows the platform for the experiment. The core control component of this platform is TMS302F28377D digital signal processor (DSP), with a control frequency set at 20 kHz. For capturing the machine's current waveform, multichannel waveform recorders MSO8204 and DS7054 are utilized. Additionally, the torque-speed meter TR-10 is used to record the machine speed and torque. The specific parameters of the prototype machine used in this experiment are given in Table I.

First, in order to compare the current dynamic response ability of vector control strategy applied in [10] (referred to as conventional VC strategy hereinafter), conventional DPCC strategy and the proposed DPCC strategy, a comparative experiment is conducted on the current step response at a speed of 1000 r/min and a load of 0.75 N·m. In the following text, i_{d_ref}, i_{q_ref}, and i_{0_ref} denote the reference values of the $dq0$-axis currents, while i_{d_fbk}, i_{q_fbk}, and i_{0_fbk} denote the feedback values of the $dq0$-axis currents. Additionally, i_a denote the current of phase A. Fig. 5(a) and (b) adopted the conventional VC strategy. When i_{q_ref} changes from 8.1 to 15.1 A, the tracking time required is 6.9 ms; when i_{0_ref} changes from 5.6 to 10.7 A, the tracking time required is 6.8 ms; when the reference current suddenly decreases, the time taken for the feedback current to track the reference current is 7.1 and 6.6 ms, respectively. When the reference current changes suddenly, the disturbance of phase current is small, and the d-axis current can also track the reference value stably.

Fig. 5(c) and (d) shows the results of adopting the conventional DPCC strategy. In the scenario where the reference current abruptly increases, the feedback current is able to swiftly track and reach the reference value within 3.2 and 5.1 ms, respectively. Conversely, when the reference current suddenly decreases, the time required for the feedback current to track the reference current is 3.2 and 5.8 ms, respectively. It can be seen that after applying the conventional DPCC strategy, the dynamic response ability of the current has been improved. Moreover, regardless of how the reference current changes, the current can accurately track the reference value in the steady state. Obviously, the use of the conventional DPCC strategy can achieve a better control effect than the conventional VC strategy. However, during the adjustment process, significant fluctuations and large inrush currents occurred in the phase current. This is because the voltage coupling component of the machine was ignored when the DPCC strategy was introduced. These phenomena will lead to an increase in system losses and shorten the service life of power electronic devices.

Fig. 5(e) and (f) shows the results of the proposed DPCC strategy. When the reference current suddenly increases, the time needed for the feedback current to follow the reference value is shorter, specifically 2.6 and 3.1 ms, respectively. Conversely, when the reference current suddenly decreases, the time required for the feedback current to track the reference current is 1.3 and 3.8 ms, respectively. Similarly, the dynamic control effect of this strategy on the current is also superior to that of the conventional VC strategy. Furthermore, compared with the conventional DPCC strategy, the dynamic adjustment time of the current of this strategy is shorter. It is worth noting that when the reference current undergoes a sudden change, the fluctuation of the phase current is minimized, making the transition smoother. This is because the proposed strategy can not only compensate for the interference caused by parameter mismatch, but also for the interference caused by the coupling phenomenon of the machine. This means that disturbances are compensated more fully and the current can be regulated more precisely during the dynamic response process.

Second, to evaluate the robustness of the two proposed strategies against parameter mismatch, the following experimental setup was used: the machine speed is adjusted to 1000 r/min, the load is set to 0.75 N·m, the resistance is increased to 0.8 times its nominal value, and both the static inductance and the primary alternating inductance are set to 1.3 times their nominal values. A comparative experiment is then conducted to observe the step response of the current. Fig. 6(a) and (b) shows the results of adopting the conventional DPCC strategy. When the reference current experiences a sudden increase, the feedback current is still able to accurately track the reference value. The time required for this tracking is 3.7 and 5.8 ms, respectively. Conversely, when the reference current suddenly decreases, the time taken for the feedback current to follow the reference value is 5.8 and 6.1 ms, respectively. In the case of parameter changes, the conventional DPCC strategy still outperforms the PI strategy in terms of the dynamic response of current. Notably, the existence of coupling amplifies the impact of disturbances caused by parameter mismatch, resulting in fluctuations in the predicted current and the calculated reference voltage, and further leading to significant fluctuations in the phase current during the regulation process.

Fig. 6(c) and (d) shows the results of the proposed DPCC strategy. When the reference current suddenly increases, the current can also be quickly tracked to the reference value, the required time is 3.4 and 5.9 ms, respectively. When the reference current suddenly decreases, the time required for accurate

$$\begin{bmatrix}\hat{i}_d(k+1)\\ \hat{i}_q(k+1)\\ \hat{i}_0(k+1)\end{bmatrix}=T_sD\begin{bmatrix}u_d(k)-Ri_d(k)+h_d(k)\\ u_q(k)-Ri_q(k)+h_q(k)\\ u_0(k)-Ri_0(k)+h_0(k)\end{bmatrix}+\begin{bmatrix}\hat{i}_d(k)\\ \hat{i}_q(k)\\ \hat{i}_0(k)\end{bmatrix}+T_s\begin{bmatrix}a_d(\hat{i}_d(k)-i_d(k))\\ a_q(\hat{i}_q(k)-i_q(k))\\ a_0(\hat{i}_0(k)-i_0(k))\end{bmatrix}-T_s\omega_e(k)DB\begin{bmatrix}i_d(k)\\ i_q(k)\\ i_0(k)\end{bmatrix} \tag{19}$$

$$\begin{cases}u_d^*(k+1)=R\hat{i}_d(k+1)+\frac{L_0}{T_s}(i_d^*(k+1)-\hat{i}_d(k+1))-L_0\omega_e(k)\hat{i}_q(k+1)-h_d(k+1)+u_{dr}(k+1)\\ u_q^*(k+1)=R\hat{i}_q(k+1)+\frac{L_0}{T_s}(i_q^*(k+1)-\hat{i}_q(k+1))+L_0\omega_e(k)\hat{i}_d(k+1)+L_1\omega_e(k)\hat{i}_0(k+1)-h_q(k+1)+u_{qr}(k+1)\\ u_0^*(k+1)=R\hat{i}_0(k+1)+\frac{L_0}{T_s}(i_0^*(k+1)-\hat{i}_0(k+1))-h_0(k+1)+u_{0r}(k+1)\end{cases}. \tag{20}$$

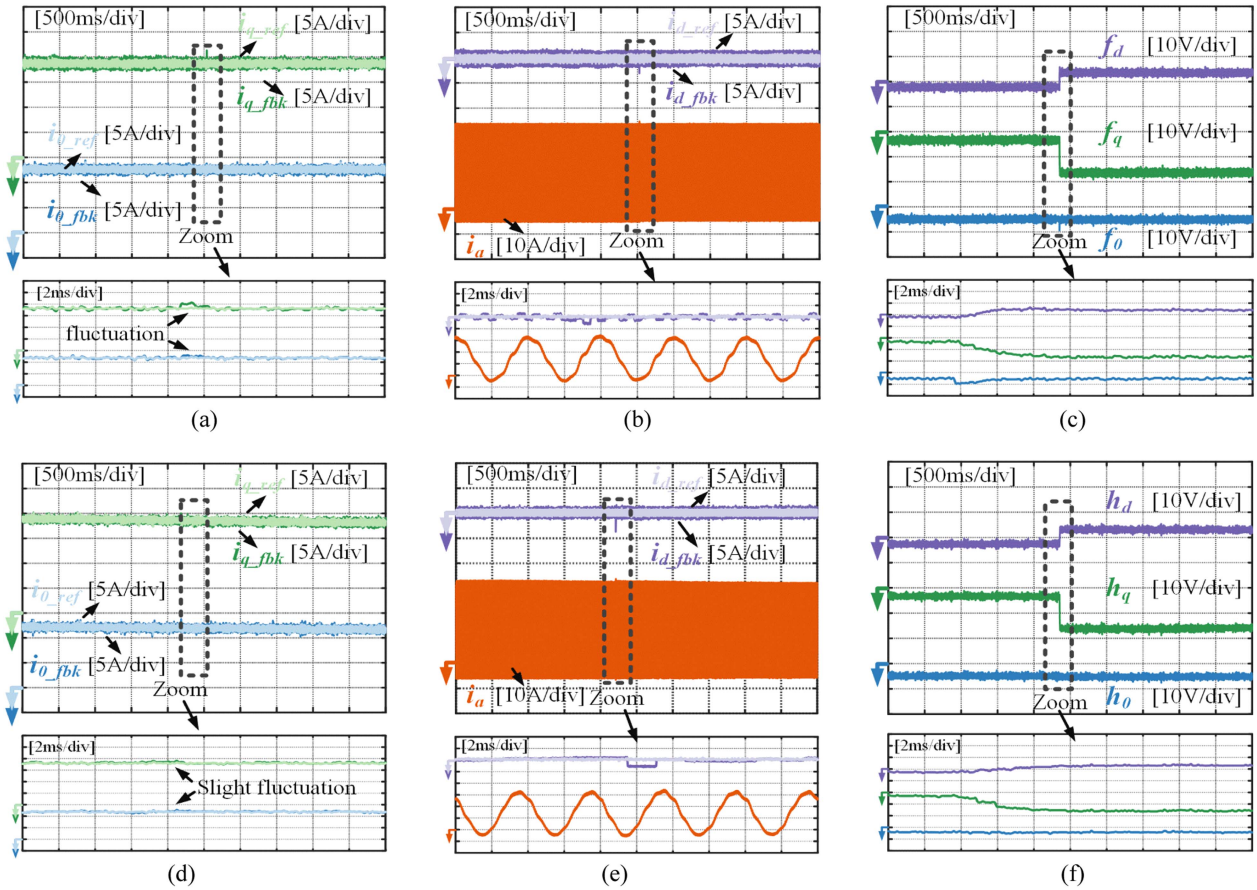

Fig. 7 Experimental results of dynamic responses of $dq0$-axis current, phase current and disturbance compensation voltage with different strategies under sudden parameter mismatch. (a) i_q and i_0 of conventional DPCC strategy. (b) i_d and i_a of conventional DPCC strategy. (c) Disturbance compensation voltage of conventional DPCC strategy. (d) i_q and i_0 of proposed DPCC strategy. (e) i_d and i_a of conventional DPCC strategy. (f) Disturbance compensation voltage of proposed DPCC strategy

current tracking is 3.3 and 3.6 ms, respectively. It can be seen that the control effect of the proposed strategy is still superior to that of the conventional VC strategy and the conventional DPCC strategy. Furthermore, due to the compensation for disturbances in the current prediction process and the voltage calculation process, when the reference current changes suddenly, the phase current only experiences very small fluctuations.

Then, the machine speed is adjusted to 1500 r/min and the load is set to 2.55 N·m. When the machine is running stably, the machine parameters in the controller are changed suddenly to observe the compensation ability of the two strategies to the disturbance. In the experiment, the resistance variation is 0.8 times of the nominal, and the static inductance and primary alternating inductance are both 1.3 times of the nominal, as shown in Fig. 7(a)–(c) shows the results of adopting the conventional DPCC strategy. When the parameters are mismatched, the $dq0$-axis current and the phase current have some disturbance. The dq0-axis disturbance voltage generated by parameter mismatch is quickly predicted and compensated, which ensures the accuracy of feedback current tracking. Fig. 7(d)–(f) shows the results of adopting the proposed DPCC strategy. Compared with the conventional control strategy, when the parameters are suddenly mismatched, the current on the dq0-axis only fluctuates slightly, indicating that the proposed control strategy has a stronger ability to resist disturbance. In addition, the proposed strategy can predict the dq0-axis disturbance voltage more smoothly and quickly.

The coupling phenomenon of dc-biased-VRM is closely related to machine parameters. Parameter mismatch not only interferes with current prediction and voltage reference calculation, but also affects the disturbance caused by coupling. Although the conventional control strategy can deal with the disturbance quickly, because the coupling phenomenon of dc-biased-VRM is not considered, the predicted disturbance has small fluctuations. The proposed strategy cannot only compensate the disturbance caused by parameter mismatch, but also compensate the disturbance caused by the coupling phenomenon, so as to predict the disturbance voltage smoothly and reduce the influence of the disturbance on the current.

Furthermore, the load variation experiment under steady state operation is also carried out. When the machine speed is stable at 1500 r/min, the load is instantaneously increased from 0.65 to 1.9 N·m. Fig. 8(a) and (b) shows the results of adopting the conventional DPCC strategy. After a sudden load change, the feedback current of the dq0-axis accurately tracks the reference current, and the q0-axis current reaches a stable state after a short

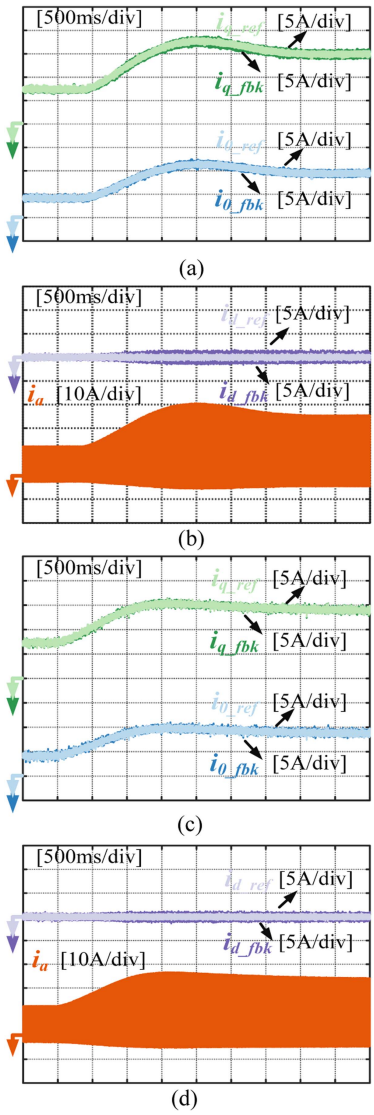

Fig. 8 Experimental results of dynamic response of $dq0$-axis current and phase current using different strategies when the load changes. (a) i_a and i_0 of conventional DPCC strategy. (b) i_d and i_a of conventional DPCC strategy. (c) i_q and i_0 of proposed DPCC strategy. (d) i_d and i_a of proposed DPCC strategy.

overshoot. Fig. 8(c) and (d) shows the results of adopting the proposed DPCC strategy. The feedback current of the $dq0$-axis in the proposed strategy accurately tracks the reference current. Also, compared with the conventional strategy, the current overshoot of $q0$-axis is smaller, which means the whole adjustment process is smoother. This is because the proposed strategy considered the coupling phenomenon between the $dq0$-axis. By implementing coupling voltage compensation, it achieves higher precision in current control and enhances the dynamic performance of the system.

The tracking times of the $d0$-axis current when the reference value increases and decreases were averaged, resulting in the comparison of current tracking times between the two control strategies presented in Table II. The condition I refers to the experimental scenario in Fig. 5, while the condition II refers to that in Fig. 6. It can be observed that the strategy proposed in this article shortens the current tracking time under different conditions, which indicates that the dynamic response capability of the system has been improved.

TABLE II
COMPARISON OF CURRENT TRACKING TIME

		Conventional Strategy	Proposed Strategy	Improvement Rate
Condition I	i_q	3.20 ms	1.95 ms	39.06%
	i_0	5.45 ms	3.45 ms	36.70%
Condition II	i_q	4.75 ms	3.35 ms	29.47%
	i_0	5.95 ms	4.75 ms	20.17%

TABLE III
COMPARISON OF PHASE CURRENT FLUCTUATIONS

	Conventional strategy	Proposed strategy	Improvement Rate
Condition I	62.41%	24.35%	60.98%
Condition II	30.39%	14.58%	52.02%

In addition, a comparison was made of the fluctuation of phase current when the current reference value changes. This ratio is calculated by dividing the difference between the value at the point of maximum phase current fluctuation and the value at the same phase under steady-state condition by the root mean square of current, as given in Table III. It can be observed that with the strategy proposed in this article, the phase current exhibits smaller fluctuations, which improves the smoothness during the current regulation process.

VI. CONCLUSION

Based on the conventional ESO-based DPCC strategy applicable to dc-biased-VRM, this article proposes an improved DPCC strategy based on ESO with coupling disturbance compensation. In the process of predicting current and disturbance, not only the disturbance caused by parameter mismatch, but also the disturbance caused by coupling phenomenon are considered. In this way, the disturbance can be compensated more accurately, which in turn enhances the precision of voltage reference calculations and further strengthens the system's dynamic response capability.

The effectiveness of the two strategies has been validated on the dc-biased-VRM experimental platform, and the superiority of the strategy proposed in this article is further verified through experiments. Compared with the conventional VC strategy and the conventional DPCC strategy, this strategy has faster current regulation ability. In addition, the dynamic regulation process is smoother and there is less disturbance in the current, which helps to improve the utilization rate of the current and reduce the impact of the current shock on the power electronic equipment.

REFERENCES

[1] J. Lu, Z. Zhang, J. Li, and H. Shi, "A single-stage control strategy of wound-rotor synchronous starter generator under excitation failure conditions for hybrid-electric propulsion aircraft application," *IEEE Trans. Transport. Electrific*, vol. 10, no. 3, pp. 5368–5378, Sep. 2024.

[2] H. Chen, G. Guan, G. Han, and H. Chen, "Fault diagnosis and tolerant control strategy for position sensors of switched reluctance starter/generator systems," *IEEE Trans. Transport. Electrific*, vol. 6, no. 4, pp. 1508–1518, Dec. 2020.

[3] Z. Yu, C. Gan, K. Ni, Y. Chen, and R. Qu, "Dual-electric-port bidirectional flux-modulated switched reluctance machine drive with multiple charging functions for electric vehicle applications," *IEEE Trans. Power Electron.*, vol. 36, no. 5, pp. 5818–5831, May 2021.
[4] S. Jia, R. Qu, W. Kong, D. Li, and J. Li, "Flux modulation principles of DC-biased sinusoidal current Vernier reluctance machines," *IEEE Trans. Ind. Appl.*, vol. 54, no. 4, pp. 3187–3196, Jul./Aug. 2018.
[5] S. Jia, R. Qu, W. Kong, D. Li, J. Li, and R. Zhang, "Stator/rotor slot and winding pole pair combinations of DC-biased current Vernier reluctance machines," *IEEE Trans. Ind. Appl.*, vol. 54, no. 6, pp. 5967–5977, Nov./Dec. 2018.
[6] Z. Yu, C. Gan, Y. Chen, and R. Qu, "DC-biased sinusoidal current excited switched reluctance machine drives based on flux modulation principle," *IEEE Trans. Power Electron.*, vol. 35, no. 10, pp. 10614–10628, Oct. 2020.
[7] Z. Yu, W. Kong, and R. Qu, "Direct torque control strategy for DC-biased Vernier reluctance machines capable of zero-sequence current regulation," *IEEE Trans. Ind. Electron.*, vol. 68, no. 3, pp. 2024–2033, Mar. 2021.
[8] X. Zhang, J. Zhao, Z. Yu, and Z. Pan, "Improved harmonic current injection control strategy for DC-biased-VRM based on current orthogonal component distribution to enhance output torque," *IEEE Trans. Power Electron.*, vol. 39, no. 10, pp. 12678–12689, Oct. 2024.
[9] Z. Li, W. Kong, Y. Cheng, and R. Qu, "An iterative learning based direct torque control strategy of DC-biased Vernier reluctance machines for torque ripple reduction," *IEEE Trans. Power Electron.*, vol. 38, no. 12, pp. 15456–15466, Dec. 2023.
[10] Z. Li, Z. Yu, W. Kong, R. Qu, and D. Li, "An accurate harmonic current suppression strategy for DC-biased Vernier reluctance machines based on adaptive notch filter," *IEEE Trans. Ind. Electron.*, vol. 69, no. 5, pp. 4555–4565, May 2022.
[11] Z. Yu, W. Kong, C. Gan, and R. Qu, "Power converter topologies and control strategies for DC-biased Vernier reluctance machines," *IEEE Trans. Ind. Electron.*, vol. 67, no. 6, pp. 4350–4359, Jun. 2020.
[12] Z. Yu et al., "Fault-tolerant control strategy of the open-winding inverter for DC-biased Vernier reluctance machines," *IEEE Trans. Power Electron.*, vol. 34, no. 2, pp. 1658–1671, Feb. 2019.
[13] C. Zhang et al., "Zero-sequence current suppression method for fault-tolerant OW-PMSM drive with asymmetric Zero-sequence voltage injection," *IEEE Trans. Ind. Electron.*, vol. 70, no. 3, pp. 2351–2362, Mar. 2023.
[14] B. Xu, Q. Jiang, W. Ji, and S. Ding, "An improved three-vector-based model predictive current control method for surface-mounted PMSM drives," *IEEE Trans. Transp. Electrific.*, vol. 8, no. 4, pp. 4418–4430, Dec. 2022.
[15] X. Sun, X. Lin, D. Guo, G. Lei, and M. Yao, "Improved deadbeat predictive current control with extended state observer for dual three-phase PMSMs," *IEEE Trans. Power Electron.*, vol. 39, no. 6, pp. 6769–6782, Jun. 2024.
[16] Y. Hu, Y. Luo, W. Hua, M. Hu, Y. Wang, and W. Yu, "Robust deadbeat predictive current sensorless control scheme for permanent magnet synchronous machine considering parameter mismatch," *IEEE Trans. Power Electron.*, vol. 40, no. 4, pp. 5846–5856, Apr. 2025.
[17] Z. Liu et al., "A modified deadbeat predictive current control for improving dynamic performance of PMSM," *IEEE Trans. Power Electron.*, vol. 37, no. 12, pp. 14173–14185, Dec. 2022.
[18] Y. Xu, S. Li, and J. Zou, "Integral sliding mode control based deadbeat predictive current control for PMSM drives with disturbance rejection," *IEEE Trans. Power Electron.*, vol. 37, no. 3, pp. 2845–2856, Mar. 2022.
[19] X. Sun, J. Cao, G. Lei, Y. Guo, and J. Zhu, "A robust deadbeat predictive controller with delay compensation based on composite sliding-mode observer for PMSMs," *IEEE Trans. Power Electron.*, vol. 36, no. 9, pp. 10742–10752, Sep. 2021.
[20] H. Zhang and X. Zhang, "A simple deadbeat predictive current control for OW-PMSM drives based on reference voltage redistribution," *IEEE Trans. Power Electron.*, vol. 39, no. 6, pp. 7362–7374, Jun. 2024.
[21] X. Yuan, C. Zhang, and S. Zhang, "A novel deadbeat predictive current control scheme for OEW-PMSM drives," *IEEE Trans. Power Electron.*, vol. 34, no. 12, pp. 11990–12000, Dec. 2019.
[22] X. Li, S. Zhang, C. Zhang, Y. Zhou, and C. Zhang, "An improved deadbeat predictive current control scheme for open-winding permanent magnet synchronous machines drives with disturbance observer," *IEEE Trans. Power Electron.*, vol. 36, no. 4, pp. 4622–4632, Apr. 2021.
[23] Z. Yu et al., "Optimal three-dimensional current computation flux weakening control strategy for DC-biased Vernier reluctance machines considering inductance nonlinearity," *IEEE Trans. Power Electron.*, vol. 34, no. 2, pp. 1560–1571, Feb. 2019.
[24] Y. Zhang, J. Jin, and L. Huang, "Model-free predictive current control of PMSM drives based on extended State observer using ultralocal model," *IEEE Trans. Ind. Electron.*, vol. 68, no. 2, pp. 993–1003, Feb. 2021.
[25] J. Lang, C. Tong, Y. Zheng, J. Bai, and P. Zheng, "Decoupled active disturbance rejection control for PMSM drives to retain deadbeat properties using composite disturbance observer," *IEEE Trans. Ind. Electron.*, vol. 71, no. 12, pp. 15445–15456, Dec. 2024.

Zixiang Yu (Member, IEEE) was born in Dalian, China, in 1993. He received the B.E.E. degree in electrical engineering from Dalian Maritime University, Dalian, China, in 2015, and the M.S. and Ph.D. degrees in electrical engineering from Huazhong University of Science &Technology, Wuhan, China, in 2018 and 2021, respectively.

Since 2021, he has been an Associate Professor in electrical engineering, with the School of Electrical Engineering and Automation, Hefei University of Technology, Hefei, China. His current research focuses on control strategy of reluctance machines, PM machines.

Xiang Zhang was born in Pingdingshan, China. He received the B.E.E. degree in electrical engineering and automation from Yangzhou University, Yangzhou, China, in 2022, and the M.Eng. degree in control engineering from Hefei University of Technology, Hefei, China, in 2025.

His research interests include control strategy of reluctance machines.

Jiwen Zhao (Senior Member, IEEE) was born in Dangshan, China. He received the Ph.D. degree in precision machinery and instrumentation from the University of Science and Technology of China, Hefei, China, in 2005.

Since 2019, he has been working with the School of Electrical and Automation Engineering, Hefei University of Technology, Hefei, China. He is currently a Professor with the School of Electrical and Automation Engineering, Hefei University of Technology, Hefei, China. His research interests include linear machine optimization design, linear machine control and photoelectric detection technology.

Yuhang Chen was born in Shandong, China. He received the bachelor's degree in electrical engineering and automation from Qingdao University, Qingdao, China, in 2023. Since 2023, he has been working toward the master's degree in electrical engineering and electrical appliances with the School of Electrical Engineering and Automation, Hefei University of Technology, Hefei., China.

His research interests include weak field control strategies for reluctance motors.

Zhenbao Pan (Member, IEEE) was born in Guilin, China. He received the B.S. degree in electrical engineering and automation and the M.S. degree in detection technology and automatic equipment from Anhui University, Hefei, China, in 2014 and 2017, respectively, and the Ph.D. degree in electrical engineering from Southeast University, Nanjing, China, in 2022.

Since 2022, he has been with Hefei University of Technology, where he is currently a Lecturer with the School of Electrical Engineering and Automation. His main research interests include design, analysis, optimization and control of permanent-magnet motors with particular reference to permanent-magnet linear motors and permanent-magnet arc motors.

Lijun Wang (Member, IEEE) was born in Chuzhou, China. He received the B.S. degree in electrical engineering and automation and the M.S. degree in detection technology and automatic Equipment from Anhui University, Hefei, China, in 2016 and 2019, respectively, and the Ph.D. degree in electrical engineering from the School of Electrical Engineering and Automation, Hefei University of Technology, Hefei, China, in 2024.

Since 2024, he has been a Lecturer with the School of Internet, Anhui University, Hefei, China. His current research focuses on linear motor control and multimotor collaborative control.